Time-lapse VSP results from the CaMI Field Research Station

Brendan J. Kolkman-Quinn and Donald C. Lawton

ABSTRACT

The Containment and Monitoring Institute operates a carbon sequestration Field Research Station (CaMI.FRS) where 15 tonnes of CO_2 have been injected between 2017 and 2019. Walk-away vertical seismic profiles (VSP) were collected in 2017, 2018, and 2019, for the purpose of time-lapse monitoring of the CO_2 plume. Two geophone and three straight-fiber DAS walk-away VSP datasets were processed. The repeatability of the time-lapse data was measured by comparing the normalized-root-mean-square and predictability values of the various datasets. High amplitude, near-offset shots resulted in large residual amplitudes and were excluded from the time-lapse results. The geophone data was found to have significantly better repeatability than the DAS data. NRMS values as low as 8%-12% were obtained for the geophone data, compared to lowest values of 21% to 29% for the DAS data. The 18m offset of the 2019-2017 geophone datasets showed a negative amplitude anomaly with positive side-lobes. This anomaly was broadly consistent with expectations of the CO_2 plume's effect on reflection amplitudes. Confidence in this interpretation was low. The anomaly was confined to one 3m binned trace in one dataset, and not far above the background residual amplitudes. No anomaly was evident in the 2019-2018 time-lapse, between which 7t of CO_2 had been injected. Applying a time-variant inverse-Q filter to the data improved vertical resolution but exacerbated amplitude residuals, worsening the repeatability metrics. Confident interpretation and characterization of the CO_2 plume will require more repeatable, consistent time-lapse results. The cause of low repeatability was attributed mainly to scaling issues between time-lapse surveys, as opposed to specific processing steps in the standard VSP workflow. Better matching of amplitudes between baseline and monitor shot gathers is critical to reducing background residual amplitudes in the time-lapse results.

INTRODUCTION

The Containment and Monitoring Institute (CaMI) operates a CO_2 sequestration project at a Field Research Station (FRS) near Brooks, AB, in western Canada. One of the monitoring technologies available at the FRS is vertical seismic profiling (VSP). Time-lapse VSPs have successfully detected CO_2 plumes at other CO_2 storage projects (Bacci et al., 2017, Cheng et al., 2010). The injection formation at the CaMI FRS is the Basal Belly River Sandstone (BBRS), a brine-saturated sandstone of approximately 10% porosity (Macquet and Lawton, 2017). The strong impedance contrast at the interface between the BBRS and the overlying coal-and shale-bearing Foremost Fm produces a strong positive seismic reflection (Figure 1). The presence of gas-phase CO_2 in the reservoir at the FRS was expected to decrease the BBRS reflection amplitude, yielding a negative residual time-lapse anomaly (Macquet and Lawton, 2017).

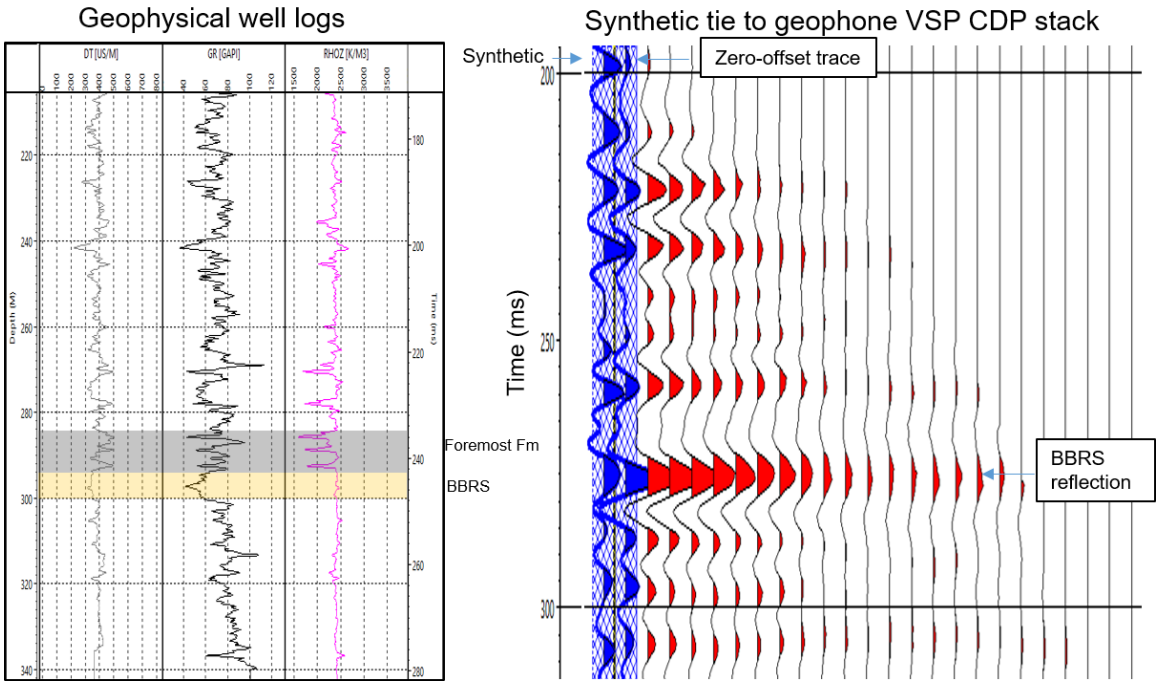

FIG. 1. Sonic, gamma ray, and density well logs with the Basal Belly River Sandstone (BBRS) highlighted in beige, and the coal-bearing Foremost Fm highlighted in grey. A synthetic trace is tied to a geophone VSP CDP stack on the right. The reflection at the interface between the Foremost Fm and BBRS produces a high amplitude, positive reflection.

A time-lapse VSP workflow was performed for the CaMI FRS using VSP data from 2017, 2018, and 2019. Processing followed a standard VSP workflow similar to previous work performed with CaMI FRS datasets (Gordon, 2019). A notable addition was the application of a time-variant inverse Q filter, whose effects were observed and measured relative to un-filtered results. Another workflow modification was a simplified depth-registration of the DAS traces, described in a later section. The objectives of this work were to establish a time-lapse processing workflow for FRS data, detect and delineate the CO_2 plume, and assess the repeatability challenges in the different datasets.

DATASETS

Observation well overview

VSPs data is collected in the geophysics observation well at the FRS. Seismic sensors include permanent downhole 3-component geophones, and both straight and helically-wound distributed acoustic sensing (DAS) fiber. Monitoring surveys have been conducted annually at the CaMI FRS since injection began in 2017. Figure 2 shows the map view of the walk-away VSP surveys processed for time-lapse purposes. Only shot locations that existed for each pair of datasets were used. There were differences in shot locations of up to 2m, but these were not found to significantly affect VSP CDP binning. Table 1 shows the total mass of CO_2 injected between the baseline and monitor surveys. The injection well is 20m north-east of the observation well, therefore the NE-SW lines were expected to be the first to detect a CO_2 anomaly around the injection well.

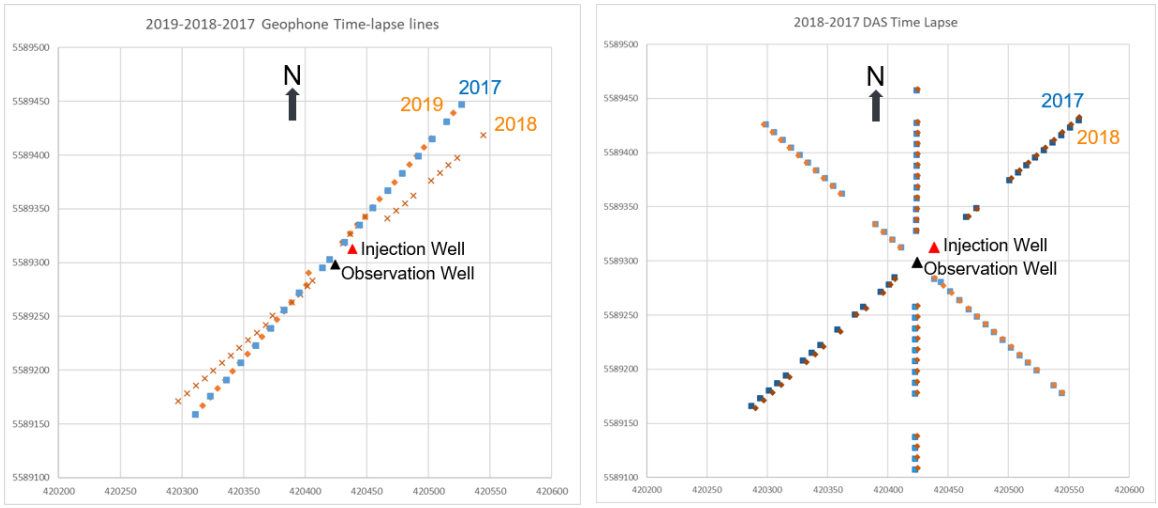

FIG. 2. Maps showing the positions of the injection well (red), observation well (black), and shot locations used for northeast-southwest walkaway VSP time-lapse. The right panel shows 20m shot spacing instead of 10, due to 2017 acquisition parameters.

Table 1. Total injected CO_2 between time-lapse surveys

Time-lapse	CO2 injected (kg)
2018-2017	8369
2019-2018	6983
2019-2017	15352

Geophones

The 24 downhole geophone array spans 190m to 305m depth at 5m intervals. Shot spacing was 20m in 2017, and 10m in 2018 and 2019. Therefore, the 2019-2017 time-lapse was done using only 20m shot intervals, while the 2019-2018 time-lapse used 10m intervals. Offsets span +/- 180m. The 2018 geophone data follows a different path than the 2017 and 2019, therefore shot locations of equal offset were considered equivalent despite sampling different reflection points in the subsurface. A 2018-2017 time-lapse was not performed as the combination of 20m spacing, different shot locations, and fewer shots in common, was deemed to be too problematic.

DAS

DAS fibers span 0m to 334m depth in the observation well. Both straight-fiber and helically-wound fiber exist in the well, but only straight-fiber was processed for this analysis. The DAS data were integrated with respect to time in order to convert from strain rate to strain. A further conversion from strain to particle velocity was not performed, therefore the DAS data are similar in waveform but are not physically equivalent to geophone data. However, as this conversion is a matter of angle-dependent scaling (Daley et al., 2015), it should be equal for both 2017 and 2018 DAS data. Therefore the exclusion of this step was not expected to significantly affect comparisons between DAS datasets.

Trace spacing was dependent on the interrogator used for data collection. The 2017 data used a Silixa interrogator with 0.25m trace spacing. 2018 data used a Fotech interrogator with 0.67m spacing. Depth registration of the DAS traces was attempted using a 2018 MEMS accelerometer dataset, which also spans the entire well. Using the method described by Gordon (2019), integrated accelerometer traces of known depth were correlated with integrated DAS traces. The accelerometer data allowed for correlation of traces from 50m to 320m. Trace spacing determined from this process matched the stock spacing given for the interrogators, within error. For example, 0.252m +/- 0.002m standard deviation agreed with the 0.25m stock trace spacing value. However, the depth assignments from this process were found to be too inconsistent, and risked introducing additional error into the time-lapse results. Therefore, depths were assigned to DAS traces by a more simplistic method:

1. The downgoing and upgoing lengths of the fiber were correlated with MEMS traces.

2. The midpoint between the downgoing and upgoing fiber traces was determined for each of the following depths: 50m, 80m, 110m, 140m, 170m, 200m, 230m, 260m, 290m, 320m. The midpoint was very consistent, +/- 0.5 traces.

3. The midpoint was assigned a depth of 330.22m, the measured depth recorded in the well schematics, adjusted for Kelly-Bushing height.

4. Using stock values of 0.25m and 0.67m (0.666666m), depths of shallower traces were calculated starting at 330.22m. The 330.22m traces were then discarded.

5. The two traces of equivalent depth were stacked together.

This depth registration method was chosen as it avoids the introduction of random error from incorrect depth assignments of each trace, while most of the systematic error introduced should cancel out during subtraction of one dataset from the other. For example, the depth of 330.22m for the midpoint traces may be incorrect, but it is incorrect for both datasets and thus will cancel out. However, the 0.25m and 0.67m trace spacing may be independently incorrect, which would introduce error in the depth registration.

DAS datasets from 2017 and 2018 were processed separately using similar workflows. As 2018 data had a 2ms sample rate and 0.67m trace spacing, different f-k filters were used compared to the 2017 data. After generating NMO-corrected prestack gathers in two-way-time (TWT), both 2017 and 2018 data were re-sampled to 2m trace spacing and 2ms time sampling. As 2m was the lowest common multiple between 0.25m and 0.67m, this effectively stacked 8 traces from 2017 or 3 traces from 2018.

METHODS AND RESULTS

VSP processing flow

In order to make stable, consistent first-break picks in the noisier DAS data, an initial f-k filter was applied to isolate the downgoing wavefield in the raw data. First breaks were picked on the filtered shot-gathers, and then re-assigned to the unfiltered raw data. Following the first break picks, processing followed a standard walk-away VSP workflow.

This workflow is described in detail for CaMI FRS datasets by Gordon (2019). Essentially, the known depths of the traces, the arrival times of the first breaks, and the known shot locations allow for isolation of the upgoing wavefield and assignment of reflections to common depth (CDPs). For geophone data, 3m CDP bins were deemed to be the limit of lateral resolution, while 2m bins were possible for the more densely sampled DAS data.

An important distinction between geophone and DAS processing is the time-variant rotation of 3-component geophone data, to maximize and separate upgoing P-wave and S-wave amplitudes. This step leads to a cleaner, higher amplitude upgoing P-wavefield in the geophone data compared to the DAS data. For DAS data, removal of the upgoing S-wavefield, and other sources of coherent noise, was done with f-k filters.

Inverse Q filter

In addition to the standard processing flow, a time-variant inverse-Q (TVIQ) filter was applied to the prestack gathers. The design and application of the filter were built-in functions of the VISTA software used for VSP processing. The process was developed from the work of Wang (2002), Hargreaves and Calvert (1991). The TVIQ process is as follows: A 1-dimensional, multilayer model of attenuation (Q) is determined using the frequency spectra of the downgoing P-wave arrivals from a near offset shot. The two-way traveltimes of each upgoing arrival determine the time spent in each constant-Q layer. Note that while amplitudes and phase are altered by the filter, high-frequencies whose amplitudes have been attenuated below the noise and whitening threshold cannot be restored (Figure 4). The TVIQ filter significantly improves vertical resolution in VSP CDP stacks (Figure 5). For comparison purposes, results in this report are given with and without the application of the TVIQ filter.

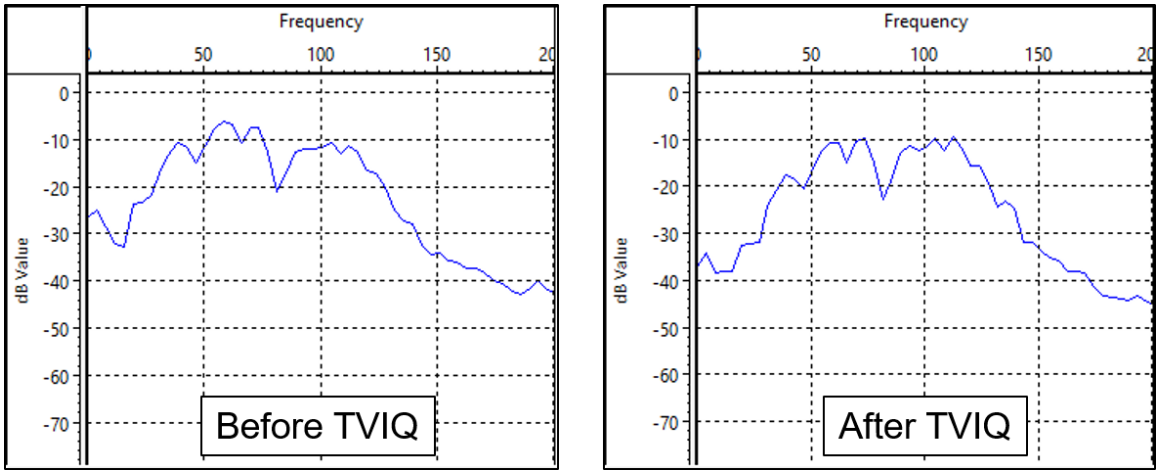

FIG. 3. Frequency spectra of the 2018 geophone VSP CDP full-stack showing the effect of the prestack inverse Q filter on the final result. The rebalancing of the frequency spectra is most evident at the -10dB mark. The inverse Q filter was applied prestack.

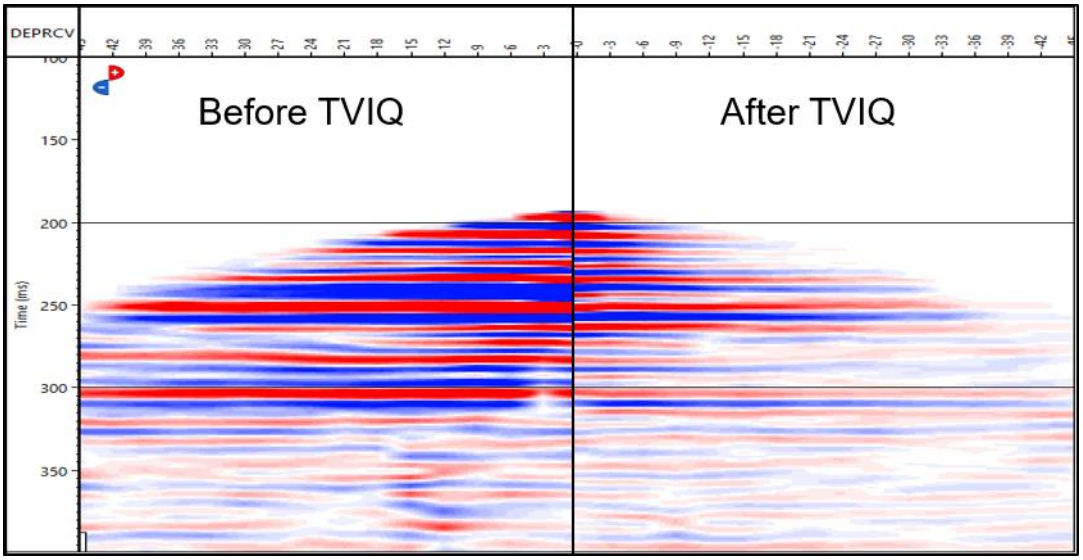

FIG. 4. Comparison of the 2018 geophone VSP CDP stack with and without the application of the time-variant inverse Q filter. The effect of restoring amplitude to the high-frequencies is a higher frequency, higher resolution result. The top of the injection interval is at 250ms.

Repeatability

Two standard metrics were used to compare the quality of the time-lapse results. The normalized root-mean-square difference (NRMS) between two seismic sections a_t and b_t is given by Equation 1:

$$NRMS = \frac{200\ RMS(a_{t-b_t})}{RMS(a_t)+RMS(b_t)}. \quad (1)$$

Expressed as a percentage from 0% to 200%, NRMS is sensitive to amplitude, phase differences, and random noise (Kragh and Christie, 2002). NRMS is minimized when the amplitude and phase difference between datasets is minimized.

Predictability (PRED) is the second repeatability metric used to evaluate the time lapse results:

$$PRED = \frac{\sum(\varphi_{ab}(t)\ \varphi_{ab}(t))}{\sum(\varphi_{aa}(t)\ \varphi_{bb}(t))}, \quad (2)$$

where φ_{ab} represents the correlation between datasets *a* and *b* over time window *t*. PRED ranges from 0% to 100% and is sensitive to lag, reflectivity differences, and random noise (Kragh and Christie, 2002). In general, PRED is consistently high for these datasets with minimal relative differences. NRMS fluctuates significantly depending on residual amplitude between datasets. PRED was calculated using only the zero lag value of the correlations.

Shaping filter

Shaping/matched filters were applied to the monitor data in order to match the baseline. A 400ms design window and 40ms operator length were used for the shaping filters. These parameters were determined through testing multiple possible values and assessing the

results visually and with NRMS and PRED. For example, a 200ms operator length led to a very close match in the noisy, 350ms-400ms time window. This indicated overly-severe changes in amplitude and phase from the shaping filter. Ideally, the design window would have excluded the zone of interest in order to avoid tampering with any amplitude or velocity pull-down effects of the CO_2 (Cheng et al., 2010). However, there was not enough shallow reflection data above the reservoir reflection to design an effective shaping filter (Figure 5). A 400ms window was therefore chosen to ensure that the bright reflection at the zone of interest did not have an outsized contribution to the correlation, while avoiding the inclusion of even deeper reflections with too low of a signal-to-noise ratio.

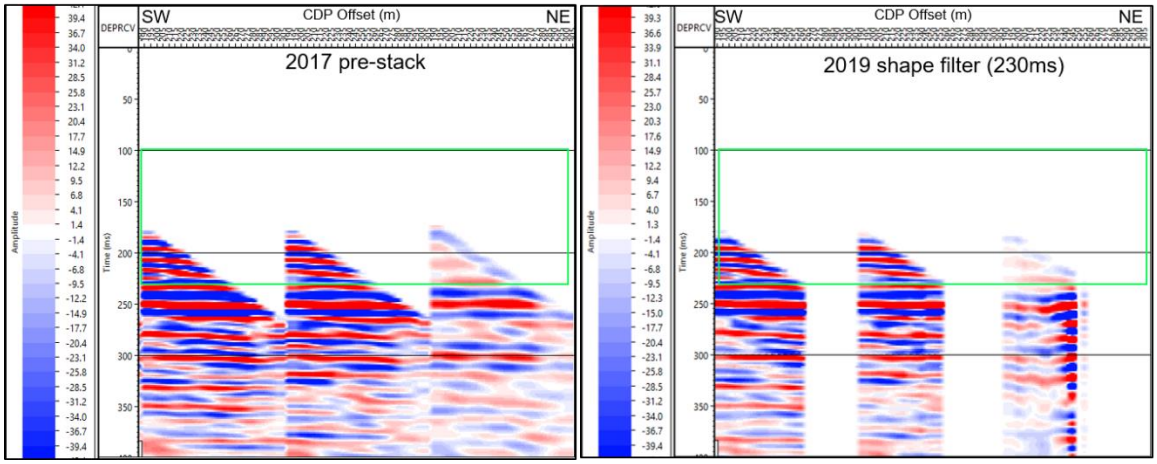

FIG. 5. Prestack geophone gathers showing a lack of shallow reflections above the 250ms reservoir reflection at the top of the BBRS. A shaping filter designed with a 230ms window (green box) excluded the reservoir but lead to data being cut-out and poorly shaped of the BBRS reflection. A 400ms shaping filter design window was used instead.

Geophone time-lapse

Figure 6 shows the result of the 2019-2017 geophone VSP time-lapse. The near-offset shot gathers were found to be poorly matched by the shaping filter, leaving large residuals (Figure 6c). These residuals prevented the interpretation of possible time-lapse anomalies. This near-offset behavior was consistent for all datasets, therefore only mid- to far-offset stacks were used in order to eliminate this problem (Figure 6d). The NRMS and PRED values of the 2019-2017 geophone time-lapse are shown in Table 2. A 0ms-400ms calculation window provided a measurement of the repeatability for the entirety of the displayed seismic sections, while a 230ms-270ms window measured repeatability around the reservoir. The best results were obtained with the 80m-180m stack, yielding NRMS of 11.8% for the 400ms window and 8.2% for the 40ms window around the reservoir. Most of the BBRS reflection amplitude has been nullified in the time-lapse difference section (Figure 6d). Negative residuals at the BBRS level in the NE section are likely due to scaling issues and not the widespread presence of CO_2. However, the green box in Figure 6d indicates a possible CO_2 amplitude anomaly at 18m offset that stands out against the background. Note that this anomaly is present in only one 3m bin, or one stacked trace. The possibility exists that the entire ~45m wide negative BBRS residual is caused by a widespread CO_2 plume. Based on modeling results by Macquet and Lawton (2017), such a widespread seismic anomaly is unlikely for a 15t injection amount.

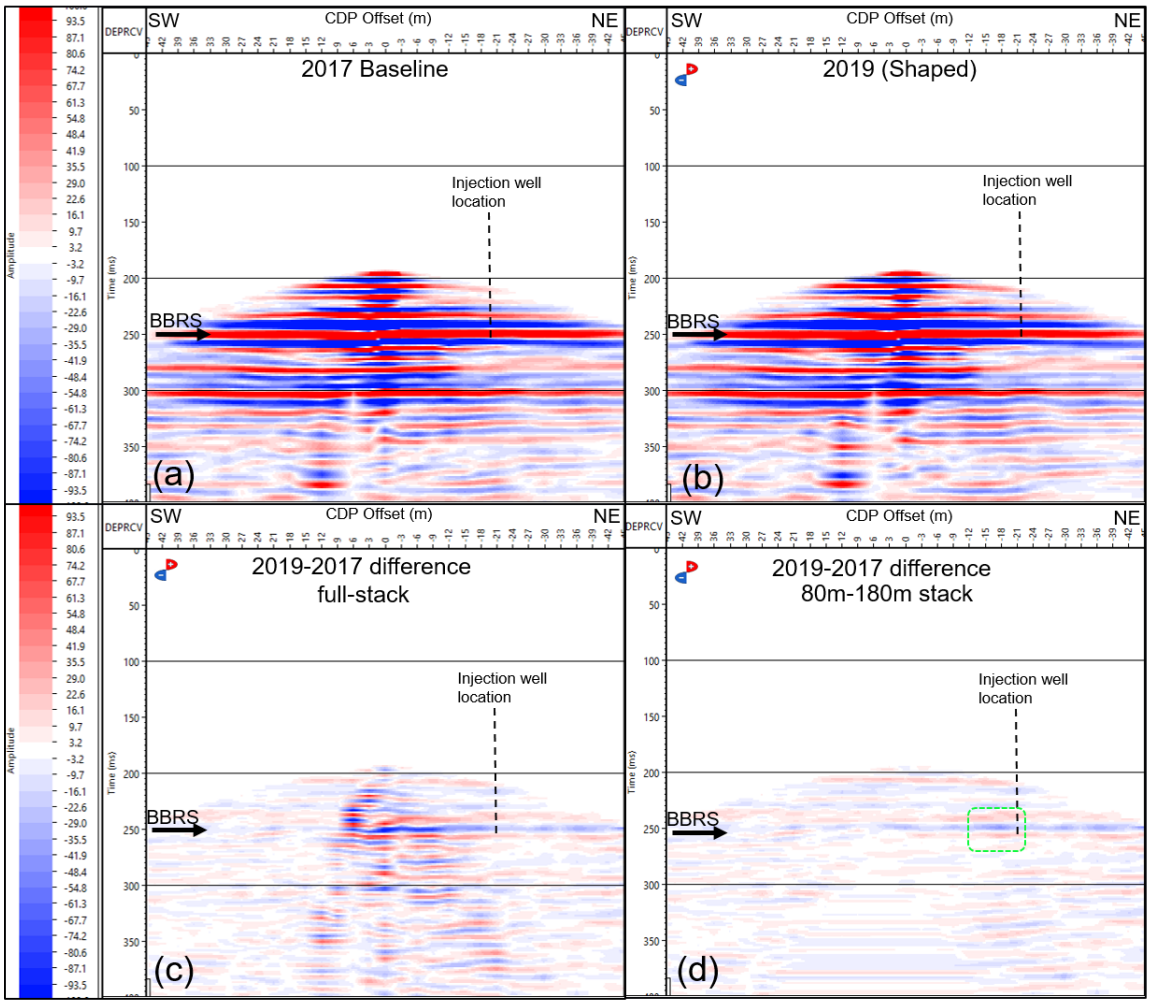

FIG. 6. Geophone time-lapse results showing (a) 2017 Baseline full-stack, (b) 2019 shape-filtered full-stack. Significant residual amplitudes exist on the full-stack time-lapse in (c). Removal of the problematic shots yielded lower residuals amplitudes (d). Green box indicates negative anomaly.

Table 2. Repeatability metrics for 2019-2017 geophone data

	0-400ms		230ms-270ms	
Version	NRMS	PRED	NRMS	PRED
Full-stack	15.6%	98.9%	12.3%	99.4%
80m-180m	11.8%	99.2%	8.3%	99.8%
Full-stack TVIQ	22.0%	98.0%	18.3%	98.7%
80m-180m TVIQ	14.4%	98.7%	10.2%	99.6%

2019-2017 time-lapse results with the time-variant inverse-Q filter applied are shown in Figure 7. The 80m-180m stack is higher frequency than in Figure 6a, but as a far-offset stack this is not visually apparent. A positive reflection at the limit of resolution combines with the BBRS peak to cause a doublet, while this reflection is more fully resolved in

Figure 4. The possible CO_2 anomaly at 18m is just as evident in Figure 7b as in Figure 6b. However, it also appears to line up with the footprint of a CDP shot gather, which is more obvious below 300ms. The NRMS and PRED values are slightly worse for the TVIQ time-lapse, as seen in Table 2.

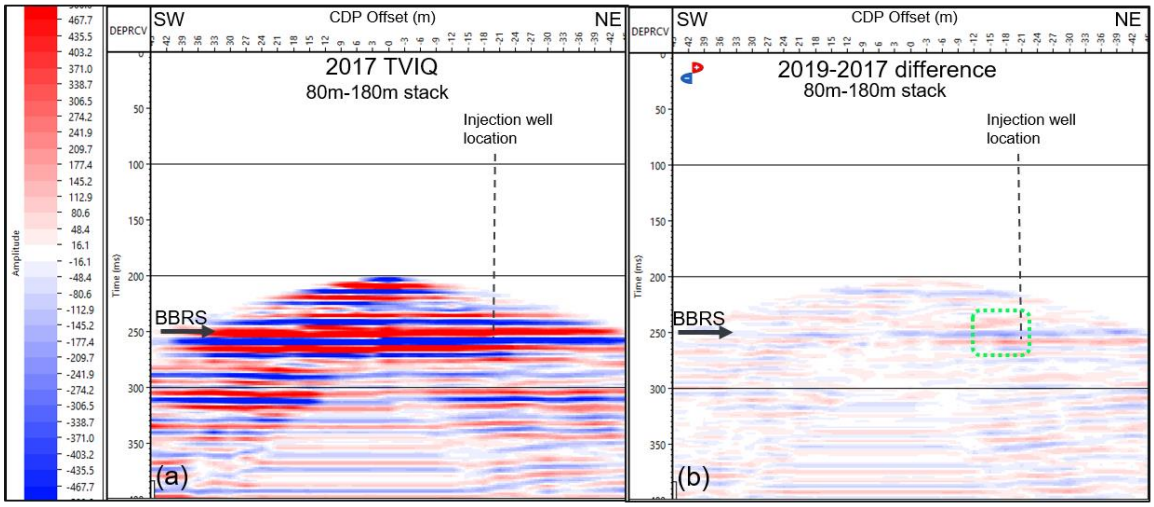

FIG. 7. Geophone 2017 baseline with TVIQ applied (a), and 2019-2017 time-lapse difference (b). Green box indicates negative amplitude anomaly.

Figure 8 shows the second geophone time-lapse result, 2019-2018. More residual amplitudes were left in the time-lapse section, with worse NRMS and PRED results in Table 3. However, the 2019-2018 result was broadly similar to the 2019-2017, increasing confidence that the processing workflow works well enough for different geophone datasets. No obvious CO2 anomaly was evident in the 2019-2018 time-lapse with or without TVIQ.

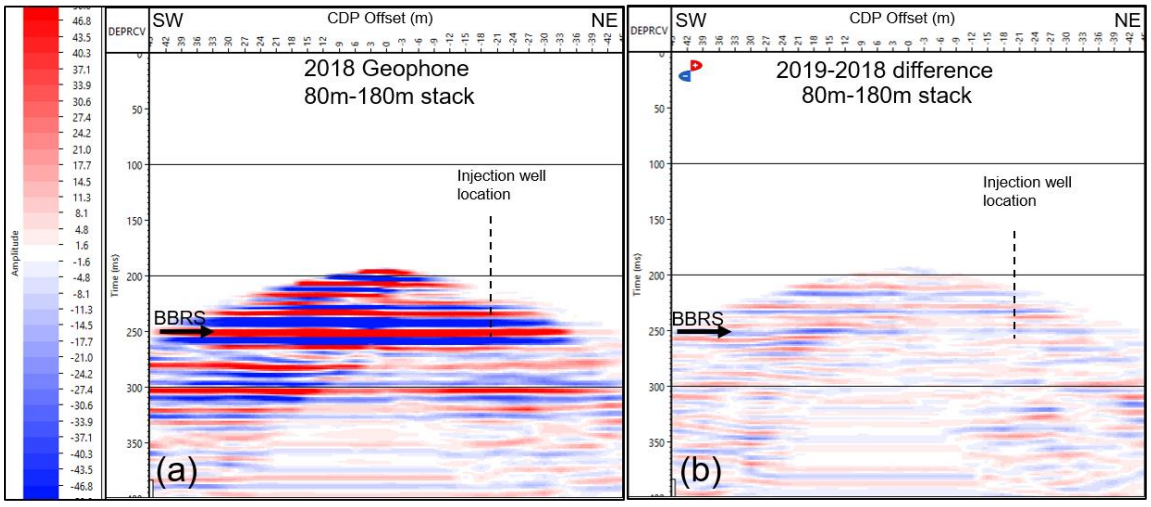

FIG. 8. The 2019-2018 geophone time-lapse result showing larger residuals than 2019-2017 but relatively good nullification of the BBRS reflection near the well. No amplitude anomaly stands out.

Table 3. Repeatability metrics for 2019-2018 geophone data

	0-400ms		230ms-270ms	
Version	NRMS	PRED	NRMS	PRED
Full-stack	16.9%	98.6%	13.1%	99.4%
80m-180m	17.8%	98.5%	12.5%	99.4%
Full-stack TVIQ	22.1%	97.7%	18.0%	98.7%
80m-180m TVIQ	23.6%	97.5%	17.7%	98.8%

DAS time-lapse

Due to the greater vertical coverage of the DAS fibers compared to the geophone array, significantly more shallow and far-offset reflections are recorded (Figure 9). It was expected that the shallow DAS data could be used to design a shaping filter down to only 230ms or 240ms, excluding the BBRS reservoir. However, the prestack data suffered similarly to the geophone data, and a 400ms design window was used once again. A poststack shaping filter attempt resulted in poor scaling, as the prestack shot gathers can have significant amplitude differences between 2017 and 2018.

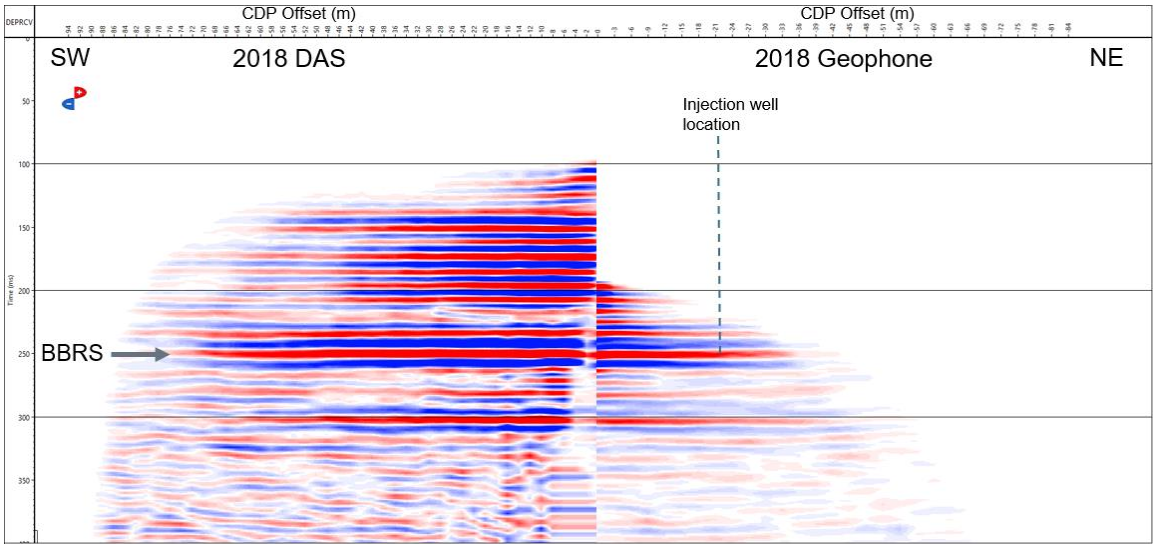

FIG. 9. Comparison between 2018 DAS and geophone VSP CDP stacks. These full-stack sections show more shallow and far-offset reflections in the DAS data, with good reflection coherence out to far offsets. Resolution of poorly resolved reflections appears better in the DAS data.

As with the geophone data, the near offset shots proved too problematic for time-lapse and were excluded. Figure 10 shows the NE half of the 2018-2017 DAS time-lapse, using 60m-190m and 110m-180m stacks. Significant residual amplitudes are apparent in the time-lapse sections, and this is confirmed by the poor NRMS results in Table 4. Note that the NRMS and PRED results were calculated for 80m offset across the entire section, not just the north-east half. However, aside from minor 1%-2% fluctuations, the calculation of NRMS and PRED was not highly influenced by the offset range. Predictability results are in Table 5.

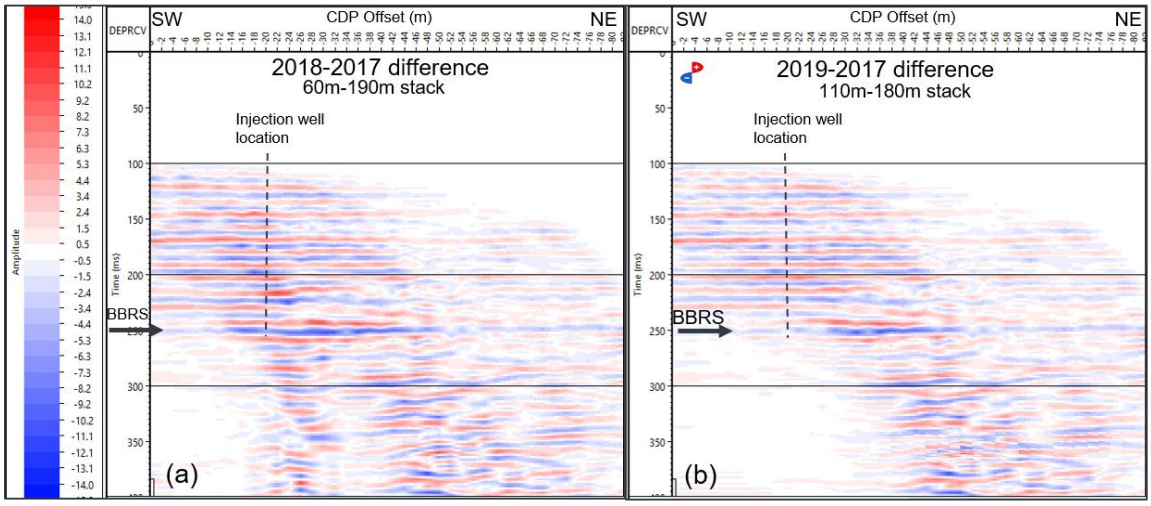

FIG. 10. DAS time-lapse results from a 60m-190m stack (a) and 110m-180m stack (b). Significant residuals exist between surveys. No CO_2 anomaly is evident at the BBRS level amongst the background residuals. Only the 0m-82m north-east half of the section is displayed.

As seen in Figure 2, two other DAS time-lapse lines were processed with north-south and northwest-southeast orientations. Although no CO2 anomaly was expected yet on those lines, they were processed in order to compare the repeatability results with the NE SW time-lapse. Due to more limited shot availability, the offsets were cut-off at 90m to provide far offset stacks with comparable fold to the NE SW lines. The NRMS and PRED values for all three DAS time-lapse lines are provided in Table 4 and Table 5.

Table 4. NRMS for three DAS time-lapse lines with and without TVIQ applied

	0ms-400ms		230ms-270ms	
Version	NRMS	NRMS TVIQ	NRMS	NRMS TVIQ
NE SW 60m-190m	39%	43%	28%	33%
NE SW 110m-190m	43%	47%	29%	35%
N S 90m-190m	38%	51%	27%	38%
NW SE 90m-180m	33%	42%	21%	28%

Table 5. PRED for 3 DAS time-lapse lines with and without TVIQ applied

	0ms-400ms		230ms-270ms	
Version	PRED	PRED TVIQ	PRED	PRED TVIQ
NE SW 60m-190m	92%	90%	96%	96%
NE SW 110m-190m	89%	88%	97%	95%
N S 90m-190m	91%	83%	96%	93%
NW SE 90m-180m	96%	89%	97%	96%

The best of the DAS time-lapse sections appears to be the NW SE line, with 21% NRMS and 97% PRED. This line is shown in Figure 11. It is clear from the seismic sections that significant residual amplitudes are being left from each reflection, indicating poor scaling

of the prestack shot gathers by the shaping filter. These DAS results will need to be improved in order to image the CO_2 plume.

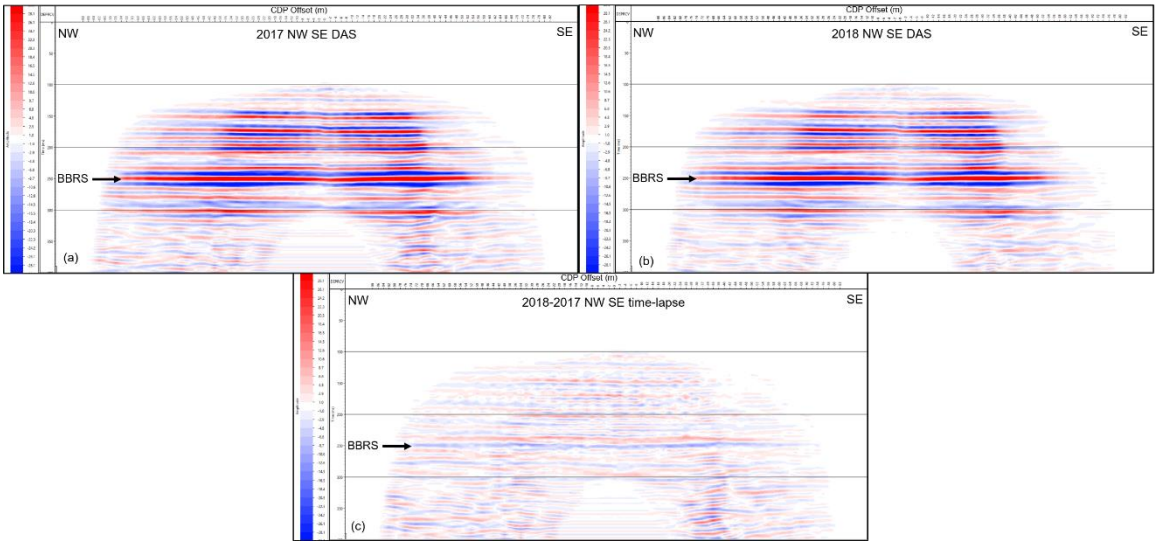

FIG. 11. DAS time-lapse result from the NW SE line. Despite having the best repeatability out of the three DAS lines, the result shows significant residuals from each reflection, indicating poor scaling by the shaping filter.

DISCUSSION

The geophone time-lapse results from the 2019-2017 and 2019-2018 lines had good repeatability, with 8%-18% NRMS for the far-offset stacks, depending on the analysis window used. The choice of windows in this report was intended to show the extremes, with intermediate values obtained for windows such as 0ms-300ms or 230ms-400ms not reported here. It is important to note that the spectral bandwidth of the VSP CDP stacks decreases with the removal of near offset shots. NRMS is sensitive to the maximum frequency of the data (K. Davies, personal communication, 2020), which decreases from ~140Hz to ~100Hz from near-offset to far-offset. Independent of near-offset amplitude scaling problems, far-offset stacks are expected to have lower NRMS values than full-stacks.

Compared to the geophone data, DAS repeatability was worse. The best DAS result came from the NW SE line with NRMS = 21% and PRED = 97%. The worst result came from the NE SW line, with NRMS = 29% and PRED = 97% over the 40ms window around the BBRS. Analysis windows of 400ms had very poor NRMS in the 33%-43% range. For reference, a 50% amplitude difference in otherwise identical datasets will cause a NRMS of 66.7% (Kragh and Christie, 2002). These high amplitude residuals from poorly scaled reflections are the main barrier to successful time-lapse with the DAS data.

The processing workflow for DAS data was designed to be similar to the geophone workflow. A notable difference being the use of an f-k filter to remove upgoing shear waves, rather than time-variant hodogram rotation. In the future, this step will be re-examined to ensure the efficacy of the f-k filter. However, this is unlikely to be the cause of the poor repeatability results. The processed, prestack DAS gathers appear visually

noisier than the geophone data, but also appear to stack together to produce VSP CDP sections that are equal or superior. Any shortcomings in the DAS processing that fail to eliminate sources of coherent noise, such as multiples or upgoing shear waves, were expected to affect both datasets equally. These consistent noise sources would then be expected to cancel out in the time-lapse subtraction.

Given the lack of randomness in the DAS time-lapse residuals, improper scaling between common shot-points is likely the greatest barrier to good repeatability. High-amplitude near-offset shots had to be removed from the analysis simply due to poor scaling. To improve the DAS results, one avenue to explore is scaling the RMS amplitudes of different shot gathers in order to achieve similar stacked amplitudes. A subsequent option would be designing the shaping filter with poststack data to make use of the shallow reflections. Alternately, designing and applying the shaping filter using CDP-converted pre-stack shot gathers may act as a compromise, with the expected loss of fewer traces than was the case in figure 5. Investigating ways to scale the relative amplitudes between the baseline and monitor surveys' shot gathers, without solely relying on the shaping filter to do so, may help reduce much of the residual amplitudes. Such a procedure would likely benefit the geophone time-lapse as well.

The time-variant inverse Q filter led to only minor increases in NRMS in the geophone data, on the order of 2% to 6% for the 80m-180m far-offset stack. For geophone and Das datasets, the TVIQ filter led to large increases in NRMS for larger initial values of NRMS. It is likely that by increasing amplitudes of the high-frequencies, the TVIQ simply exacerbates existing noise and scaling problems between datasets. The TVIQ process is still expected to improve vertical resolution of the reservoir interval, and will continue to be tested with future datasets. To reduce uncertainty, a more robust, generalized model can be created using multiple near-offset shots to determine the attenuation-depth model, rather than one shot.

CONCLUSIONS

Two geophone and three DAS walk-away VSP datasets were processed for time-lapse analysis of the CaMI FRS CO_2 sequestration project. The repeatability of the time-lapse data was measured by comparing the normalized-root-mean-square and predictability values of the various datasets. Near-offset shots were poorly scaled compared to far offset shots, therefore only shot offsets within 60m-190m were used. The geophone data was found to have significantly better repeatability than the DAS data, with NRMS as low as 8%-12% in a window around the reservoir interval. The 18m offset of the 2019-2017 geophone datasets showed a negative amplitude anomaly with positive side-lobes in the vicinity of the injection well. 15t of CO_2 had been injected during that period. Although this anomaly was consistent with expectations of the CO_2 plume's effect on reflection amplitudes, it was not confirmed in other datasets. NRMS values for DAS datasets were high, between 21% and 43% depending on the time-window examined. These large NRMS values were attributed to poor scaling between shot gathers, with large non-random residuals apparent in the time-lapse difference sections. Confident interpretation and characterization of the CO_2 plume will require more repeatable, consistent time-lapse results. Better matching of amplitudes between baseline and monitor shot gathers is crucial. Processing the 2020 survey data will provide more time-lapse datasets, with greater

injection amounts between surveys. With several generations of time-lapse data, iterative improvements are expected in the time-lapse processing workflow for CaMI FRS datasets.

ACKNOWLEDGEMENTS

This work was funded by CREWES industrial sponsors, NSERC (Natural Science and Engineering Research Council of Canada) through the grants CRDPJ 461179-13 and CRDPJ 543578-19. Partial funding also came from the Canada First Research Excellence Fund. The data were acquired at the Containment and Monitoring Institute Field Research Station in Newell County AB, which is part of Carbon Management Canada.

REFERENCES

Bacci, V., O'Brien, S., Frank, J., and Anderson, M., 2017, Using a walk-away DAS time-lapse VSP for CO_2 plume monitoring at the Quest CCS project: CSEG Recorder, **42**, no. 3, 18-22

Cheng, A., Huang, L., and Rutledge, K., 2010, Time-lapse VSP data processing for monitoring CO_2 injection: The Leading Edge, **29**, 196-199

Daley, T., Miller, D., Dodds, K., Cook, P., and Freifeld, B., 2015, Field testing of modular borehole monitoring with simultaneous distributed acoustic sensing and geophone vertical seismic profiles at Citronelle, Alabama: Geophysical Prospecting, **64**, 1318-1334

Gordon, A., 2019, Processing of DAS and geophone VSP data from the CaMI Field Research Station: M.Sc. Thesis, Univ. of Calgary.

Hargreaves, N.D., and Calvert, A.J., 1991, Inverse Q filtering by fourier transform: Geophysics, **56**, 519-527

Kragh, E., and Christie, P., 2002, Seismic repeatability, normalized rms, and predictability: The Leading Edge, **21**, 640-647

Macquet, M., and Lawton, D., 2017, Reservoir simulations and feasibility study for seismic monitoring at CaMI.FRS: CREWES Research Report, **29**, 56.1-56.26

Wang, Y., 2002, A stable and efficient approach of inverse Q filtering: Geophysics, **67**, 657-663